SYNAPSE 61:469–477 (2007)

Quantification of Serotonin 5-HT_{1A} Receptors in Humans With [^{11}C](*R*)-(−)-RWAY: Radiometabolite(s) Likely Confound Brain Measurements

XIANG-YANG ZHANG, FUMIHIKO YASUNO, SAMI S. ZOGHBI, JEIH-SAN LIOW, JINSOO HONG, JULIE A. McCARRON, VICTOR W. PIKE, AND ROBERT B. INNIS*

Molecular Imaging Branch, National Institute of Mental Health, National Institutes of Health, Bethesda, Maryland

KEY WORDS PET; kinetic analysis; serotonin 5-HT_{1A}; [^{11}C](*R*)-(−)-RWAY; human

ABSTRACT [^{11}C](*R*)-(−)-RWAY has been shown to be a promising radioligand for imaging brain 5-HT_{1A} receptors with positron emission tomography in rodents and nonhuman primates. We now report the first use of [^{11}C](*R*)-(−)-RWAY in six healthy human subjects, using kinetic brain imaging and serial arterial measurements of plasma parent radiotracer. At 80 min after radiotracer injection, activity ratios were about three for brain receptor-rich regions compared with cerebellum. However, the washout from brain was unexpectedly slow relative to plasma clearance of the parent radiotracer. This disparity between brain and plasma activity was quantified with distribution volume calculated from increasingly truncated brain imaging data. In both receptor-rich regions and cerebellum, distribution volumes were unstable and increased continuously from 90 to 150 min by about 30%. This increasing distribution volume was unlikely due to the variations or errors of plasma input at later time points, since a similar truncation of plasma time points from 150 to 90 min did not significantly affect the analysis of the brain data. When the metabolites of [^{11}C](*R*)-(−)-RWAY in human and monkey were compared, a moderate lipophilic radiometabolite was present at a significantly higher percentage of total plasma radioactivity in human than in monkey. The relatively slow washout of activity from brain and the temporal instability of distribution volume likely reflect the accumulation of radiometabolite(s) in human brain. Although prior studies in rodents and nonhuman primates showed [^{11}C](*R*)-(−)-RWAY to be a promising radiotracer, we suspect that a species difference in metabolism caused this serious deficiency in humans. **Synapse 61:469–477, 2007.** Published 2007 Wiley-Liss, Inc.†

INTRODUCTION

An important breakthrough for imaging 5-HT_{1A} receptors was the ^{11}C-labeling of the potent and selective antagonist WAY-100635 to provide the first successful radioligand for this neurotransmitter target (Pike et al., 1995). The radiolabel was initially placed in the *O*-methyl position (Fig. 1B). The ligand is primarily metabolized by amide hydrolysis to the amine [^{11}C]WAY-100634, which also has high affinity for 5-HT_{1A} receptors and confounds the measurement of parent radioligand binding (Osman et al., 1998). Labeled in the carbonyl position, [*carbonyl*-^{11}C]WAY-100635 does not generate the confounding metabolite [^{11}C]WAY-100634 and provides high contrast images of 5-HT_{1A} receptor distribution in brain (Pike et al., 1996). Although [*carbonyl*-^{11}C]WAY-100635 is arguably one of the best available agents to image 5-HT_{1A} receptors, it also has moderate limitations. First, radiolabeling in the carbonyl position is significantly more difficult than *O*-methylation. Second, the contrast of the images may be paradoxically too high, with uptake in cerebellum too low. Reference tissue

Contract grant sponsor: NIMH; Contract grant number: Z01-MH002795-04.

*Correspondence to: Robert B. Innis, M.D., Ph.D., Molecular Imaging Branch, National Institute of Mental Health, National Institutes of Health, Building 1, Room B3-10, One Center Drive, Bethesda, Maryland 20892-0135, USA. E-mail: robert.innis@nih.gov

Received 28 September 2006; Accepted 30 December 2006

DOI 10.1002/syn.20392

Published online in Wiley InterScience (www.interscience.wiley.com).

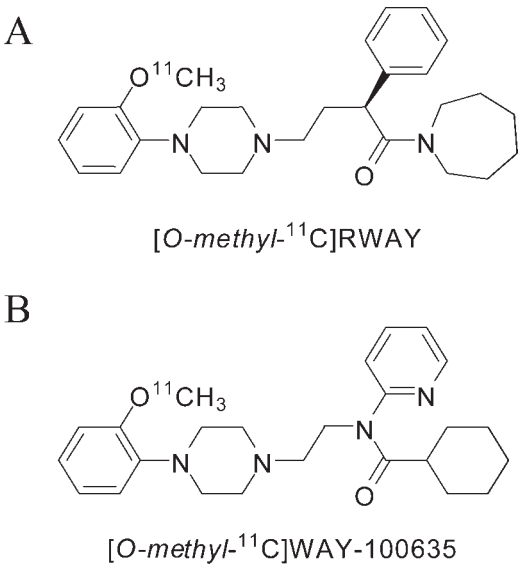

Fig. 1. Structures of [*O-methyl*-^{11}C]WAY-100635 and [*O-methyl*-^{11}C](*R*)-(−)-RWAY.

analysis calculates the ratio of brain uptake in receptor-rich to receptor-devoid regions. In the case of [*carbonyl*-^{11}C]WAY-100635, the denominator (cerebellar activity) is so low that the ratio is vulnerable to significant measurement error (Gunn et al., 1998).

A closely related analog [^{18}F]FCWAY (*trans*-4-fluoro-*N*-{2-[4-(2-methoxyphenyl)piperazin-1-yl]ethyl-*N*-(pyridin-2-yl)cyclohexanecarboxamide) is a longer lived alternative to ^{11}C-labeled analogs (Lang et al., 1999). Unfortunately, [^{18}F]FCWAY undergoes significant defluorination in humans with marked uptake of [^{18}F]fluoride in bone (Giovacchini et al., 2005). The high radioactivity in skull confounds the accurate quantitation of underlying neocortex.

In summary, each of the two most commonly used positron emission tomography (PET) tracers for the 5-HT_{1A} receptor has at least one significant deficiency. [*carbonyl*-^{11}C]WAY-100635 is difficult to synthesize and has very low uptake in cerebellum. [^{18}F]FCWAY undergoes defluorination and generates significant radioactivity in skull. We sought to develop an improved PET ligand that was resistant to amide hydrolysis, that used ^{11}C as label and thereby avoided defluorination, and that was easily labeled in a methyl position. Based on animal studies, [^{11}C](*R*)-(−)-RWAY (Fig. 1A, [^{11}C]2, 3, 4, 5, 6, 7-hexahydro-1{4-[1[4-(2-methoxyphenyl)-piperazinyl]]-2-phenylbutyryl}-*1H*-azepine) fulfills these three criteria. First, [^{11}C](*R*)-(−)-RWAY is labeled in a methyl position. Second, [^{11}C](*R*)-(−)-RWAY has a "reversed" amide linkage (and thus the term R(reverse)WAY) that is resistant to hydrolysis. Mass spectrometry studies in rats have confirmed the metabolic stability of the amide bond in RWAY (Shetty et al., 2005). Third, PET imaging in nonhuman primates with [^{11}C](*R*)-(−)-RWAY shows that it readily enters brain with a regional distribution and pharmacological displacement appropriate for binding to 5-HT_{1A} receptors (Yasuno et al., 2006). Furthermore, postmortem studies in rodents showed minimal accumulation of radiometabolites in brain (Liow et al., 2007). In addition, distribution volume measurements in nonhuman primates are very stable 70 min after tracer injection, consistent with the lack of accumulation of radiometabolites in brain (Yasuno et al., 2006). Thus, preclinical studies showed that [^{11}C](*R*)-(−)-RWAY is a promising radiotracer, and we now report the first in human use of [^{11}C](*R*)-(−)-RWAY. Unlike the results in animals, this tracer showed the serious flaw of temporal instability of distribution volume measurements, suggestive of the accumulation of radiometabolite(s) in human brain.

MATERIALS AND METHODS

Subjects

The Radiation Safety Committee of the NIH and the Institutional Review Board of the National Institute of Mental Health approved the use of [^{11}C](*R*)-(−)-RWAY in human subjects. Four male and two female healthy volunteers (age, 29 ± 10 years; range, 22–47 years; weight, 88 ± 27 kg) participated in the protocol. These and subsequent data are expressed as the mean ± SD, unless otherwise noted. Subjects gave informed, written consent and then completed a screening assessment no more than 3 months before their PET scan. The assessment included a history, physical examination, electrocardiogram (ECG), and standard blood and urine analyses to ensure that subjects were free of medical and neuropsychiatric illnesses. The laboratory tests included a complete blood count, serum chemistries, thyroid function test, urinalysis, urine drug screen, as well as syphilis, HIV, and hepatitis B screenings. About 24 h after the administration of the tracer, subjects returned to repeat the complete blood count, serum chemistries, and urinalysis.

Radiopharmaceutical preparation

Details of radiosynthesis are presented in our previous papers (Liow et al., 2007; Yasuno et al., 2006). All radioligands were radiochemically (99–100%), chemically (90–100%), and enantiomerically (100%) pure.

PET data acquisition

Both a preinjection transmission scan and a series of dynamic emission scans were acquired using a GE Advance tomograph (GE Health Care, Waukesha, WI). [^{11}C](*R*)-(−)-RWAY was administered over ~60 s, with injected activity of 664 ± 104 MBq, specific activity of 124 ± 149 GBq/μmol, and mass dose of

carrier of 5.3 ± 3.4 μg. Dynamic scans of 120 min (33 frames) were acquired in the first two subjects, whereas longer scans of 150 min (39 frames) were acquired in the subsequent four subjects.

Eight arterial blood samples were taken during the initial 2 min after the tracer injection, followed by seven samples during the next 18 min, and once every 15 min there after until 150 min. Each blood sample was separated into plasma and blood cell fraction by centrifugation. The parent tracer, separated from radiometabolites was measured as previously described (Zoghbi et al., 2006).

Radioactivity in brain and plasma were expressed as %SUV (standardized uptake value), which normalizes for injected dose and body weight.

$$\%\text{SUV} = (\%\ \text{injected activity/cm}^3\ \text{tissue}) \times (\text{g body weight})$$

Image analysis

A T1-weighted MRI was acquired for each subject in coronal orientation on a GE Signa 1.5 T scanner (SPGR, TR/TE/flip angle = 13.1 ms/5.8 ms/45°, voxel size = 0.4 × 0.4 × 1.5 mm^3).

For coregistration, a summed PET image was coregistered to the MRI scan of the same subject using a linear registration tool (FMRIB Software Library, Oxford, UK). For spatial normalization, each subject's MRI was also coregistered with respect to a T1 template (Collins et al., 1994). The two transformations were then combined and used to resample all frames of the dynamic PET images into the template space. Four regions of interest were manually defined on summed coronal PET images from 30 min to the end of study, with reference to the subject's coregistered MRI. The four regions of interest were prefrontal cortex (5.9 cm^3), temporal cortex (4.9 cm^3), hippocampus (1.7 cm^3), and cerebellum (4.0 cm^3). The cerebellar volume of interest did not include the vermis, which contains a modest density of 5-HT$_{1A}$ receptors (Parsey et al., 2005). Because all PET images were spatially normalized to a common template, the four regions of interests were applied directly to other subjects with only minor adjustment. This approach eliminated the variability due to size and shape difference of the delineated region of interests across subjects.

Estimation of distribution volume with arterial input function

Regional radioactivity data were analyzed with both standard one- and two-tissue compartment models (Cunningham and Lammertsma, 1995), using the metabolite-corrected plasma input function. Rate constants were estimated with weighted least squares and the Marquardt optimizer.

Distribution volume is the ratio at equilibrium of brain activity to the concentration of parent radiotracer in plasma (free plus protein bound). Since we used brain radioactivity, the values represent "total" distribution volume, reflecting both specific and nondisplaceable uptake. We defined distribution volume V and specific distribution volume (BP_1) as follows:

$$\text{One-tissue}: \quad V = \frac{K_1}{k_2}$$

$$\text{Two-tissue}: \quad V = \frac{K_1}{k_2}\left(\frac{1+k_3}{k_4}\right) \quad \text{BP}_1 = \frac{K_1 k_3}{k_2 k_4}$$

where K_1 and k_2 are the rate constants of transfer into and out of the brain; k_3 and k_4 are the rate constants of association and dissociation of the tracer–receptor complex, respectively.

Time stability of parameter estimates

For the four subjects with 150-min imaging data, we examined the relationship between parameter estimates and scan duration by increasingly truncating brain data sets from 0–150 to 0–30 min. Distribution volumes (V) for both temporal cortex and cerebellum, and BP_1 for temporal cortex were estimated with two-tissue compartment models. To estimate distribution volume ratio without arterial blood sampling, the data were also analyzed with the multilinear reference tissue model (MRTM) (Ichise et al., 2003). The latter method estimates binding potential (BP), which is the ratio at equilibrium of specific binding to nondisplaceable uptake.

The estimated parameters were compared with that obtained using the complete 150-min data set. The solution was considered stable after time t if the result was within 10% of that from the entire data set (i.e., 0–150 min). Image analysis and compartmental modeling were performed with PMOD software (PMOD Technologies, Adliswil, Switzerland).

Effect of later plasma data on distribution volume

The relationship of distribution volume and the duration of plasma input was analyzed by increasingly truncating plasma data from 0–150 to 0–30 min. The plasma input was fitted with three-exponential curve using the software program PMOD 2.65 (PMOD Technologies). The area under the curve (AUC) of plasma input was calculated as follows:

$$C(t) = \sum_1^3 A_i\ e^{-\lambda_i t}$$

$$\text{AUC} = \int_0^\infty C(t) = \sum_1^3 \frac{A_i}{\lambda_i}$$

where C is the concentration of parent radiotracer in plasma (free plus protein bound), A_i is the extrapo-

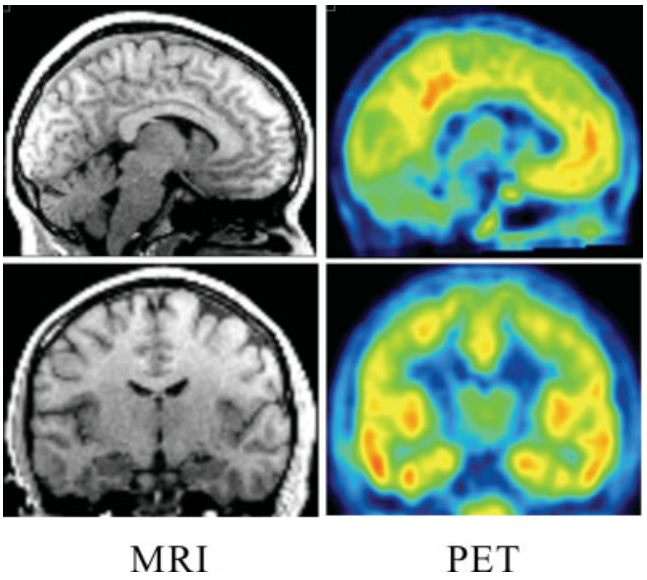

Fig. 2. Activity of [^{11}C](*R*)-(−)-RWAY in human brain. Summed PET images are on the right, and the corresponding MR images are on the left. The sagittal and coronal brain sections are located in the upper and lower panel, respectively.

lated intercept of three exponential phases, and λ_i are the three exponential rate constants. Distribution volumes for temporal cortex and cerebellum were then estimated using the two-tissue compartment model and increasingly truncated plasma data.

Statistical analysis

Goodness-of-fit by nonlinear least squares analysis was evaluated using the model selection criterion (MSC), which is a modification of the Akaike information criterion (Akaike, 1974). MSC gives greater values for better fitting. Goodness-of-fit by one-tissue and two-tissue compartmental models was compared with *F* statistics (Hawkins et al., 1986).

The standard errors of nonlinear least squares estimation for rate constants were given by the diagonal of the covariance matrix (Carson, 1986) and expressed as a percentage of the rate constants (coefficient of variation, %COV). In addition, %COV of distribution volume was calculated from the covariance matrix using the generalized form of error propagation equation (Bevington and Robinson, 2003), where correlations among parameters were taken into account.

RESULTS

Pharmacological effects of [^{11}C](*R*)-(−)-RWAY

The injected mass of carrier ligand (5.3 ± 3.4 μg) given with radioligand caused no significant changes in vital signs, ECG, or blood and urine tests, and the volunteers reported no subjective effects.

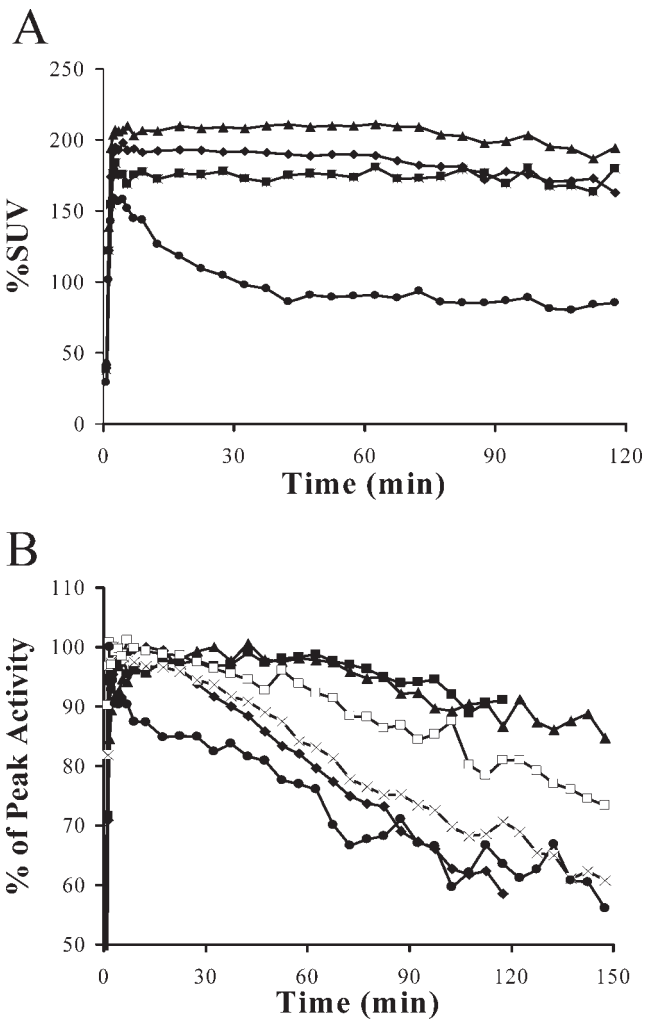

Fig. 3. **A:** Time course of regional brain activities after injection of [^{11}C](*R*)-(−)-RWAY. Activity is shown as %SUV (standardized uptake value), which normalizes for injected dose and body weight. This subject had the slowest washout of activity from brain. Prefrontal cortex (▲); temporal cortex (◆); hippocampus (■); cerebellum (●). **B:** Comparison of temporal cortex time activity curves in six subjects after injection of [^{11}C](*R*)-(−)-RWAY. Activity was normalized as % of peak activity. Lines represent the temporal cortex time activity curves from the six subjects.

Brain activity of [^{11}C](*R*)-(−)-RWAY

Brain activity of [^{11}C](*R*)-(−)-RWAY was highest in temporal cortex, prefrontal cortex, and hippocampus and low in cerebellum (Fig. 2). Brain activity of [^{11}C](*R*)-(−)-RWAY in 5-HT$_{1A}$ receptor-rich regions was about 3-fold greater than that of 5-HT$_{1A}$ receptor-poor region cerebellum at 80 min after tracer injection. However, brain activity washed out slowly (Fig. 3A) and with variable rates among the six subjects (Fig. 3B).

Arterial plasma analysis

Plasma activity of parent [^{11}C](*R*)-(−)-RWAY peaked at about 1.5 min and decreased to 4.7% ± 1.0% of the

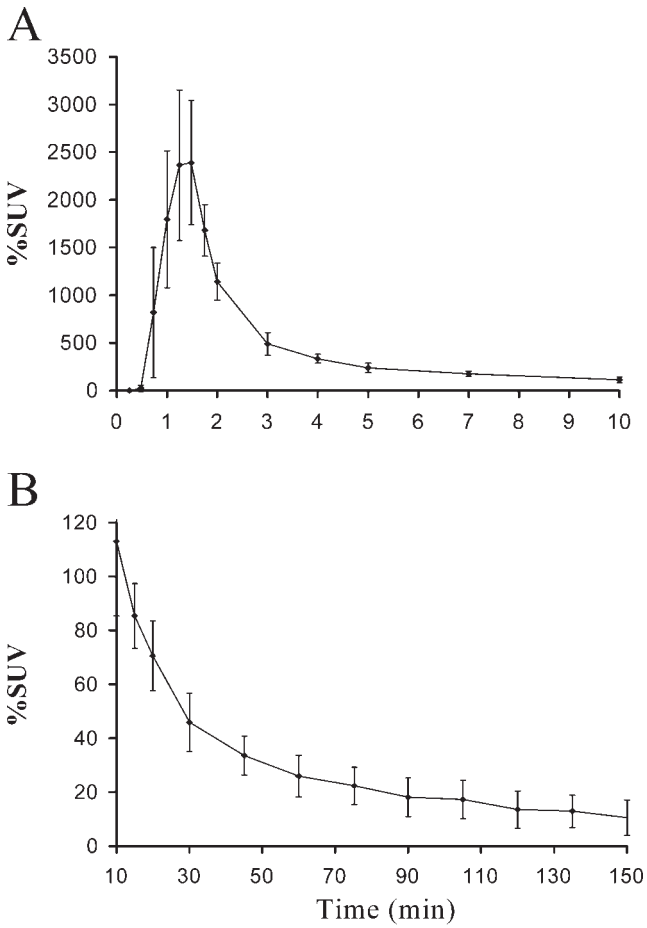

Fig. 4. Plasma activity of parent [^{11}C](*R*)-(−)-RWAY; $n = 6$. **A:** Plasma activity of parent [^{11}C](*R*)-(−)-RWAY from 0 to 10 min. **B:** Plasma activity of parent [^{11}C](*R*)-(−)-RWAY from 10 to 150 min.

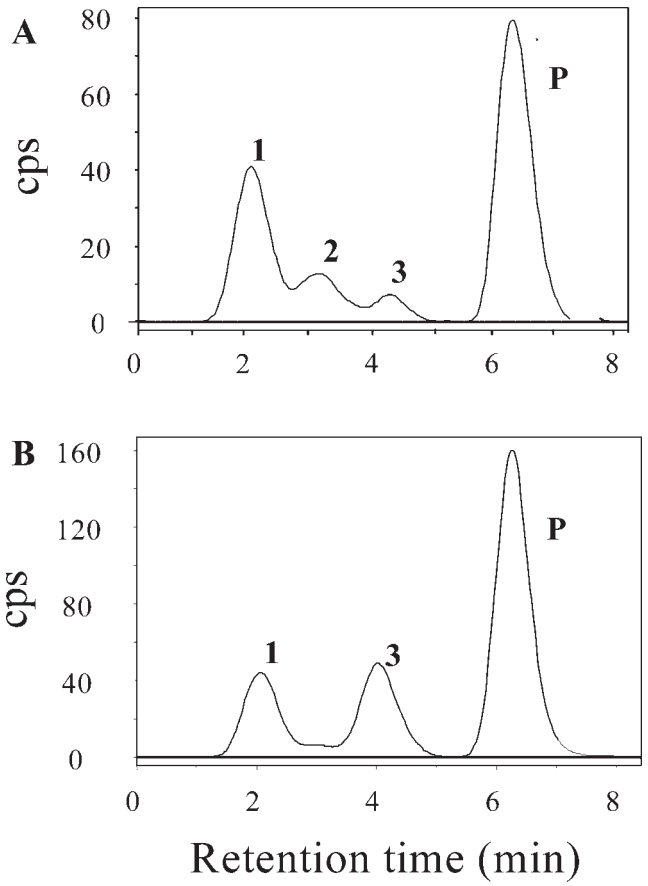

Fig. 5. **A:** Radiochromatogram of monkey arterial plasma sample obtained at 10 min after the iv injection of [^{11}C](*R*)-(−)-RWAY. Peak **3** is the most lipophilic radiometabolite, eluted in the void volume of the HPLC column. **B:** Radiochromatogram of 10 min human arterial plasma showing a polar radiometabolite peak **1** and one intermediate radiometabolite peak **3**, which occurred immediately before the parent radioligand.

peak by 10 min (Fig. 4A). The plasma activity of parent [^{11}C](*R*)-(−)-RWAY at 90 and 150 min represented 0.7% ± 0.2% and 0.4% ± 0.2% of the peak activity, respectively (Fig. 4B).

We used high-performance liquid chromatography (HPLC) and on-line radiation detection to compare the distribution of radiometabolites in human and monkey plasma. The monkey data came from a prior study (Yasuno et al., 2006), although these specific data from radiochromatography were not presented. Figure 5 provides data from a typical human and monkey plasma sample 10 min after tracer injection. While the monkey showed three radiometabolites in plasma, humans showed only two. A monkey plasma sample (Fig. 5A) was composed of a polar peak **1** (43.1%) and two minor intermediates but more lipophilic ones: peak **2** (3.7%) and peak **3** (3.2%). The [^{11}C](*R*)-(−)-RWAY, peak **P** ("parent"), was 50% of plasma activity. A human plasma sample (Fig. 5B) was composed of two radiometabolites, a polar peak **1** (19.0%), a more lipophilic peak **3** (20.6%), and the parent peak **P** (60.4%). In spite of the monkey's more extensive metabolism of 50% of the parent radioligand, radiometabolite **3** was only 3.2% of the total monkey plasma activity. In contrast, human plasma showed less metabolism of the parent peak **P** (60.4%) and a higher percentage of radiometabolite **3** (20.6%). To examine generalizability of this finding, we compared the percentage of radiometabolite **3** at 10 min after tracer injection in the six human subjects of this report with that in three monkeys previously studied with [^{11}C](*R*)-(−)-RWAY (Yasuno et al., 2006). The relatively lipophilic metabolite **3** was 13.6% ± 6.4% of total plasma activity in human compared with 5.9% ± 3.1% in monkey. This difference was significant by two-tailed *t* test ($P < 0.05$).

Nonlinear least squares compartmental analyses

Convergence was achieved in all regions and all subjects with both one- and two-tissue compartment analyses. The two-tissue compartment model provided

TABLE I. Parameter estimates (mean ± SD) obtained from the two-tissue compartmental model

Region	% COV					
	K_1 (mL cm^{-3} min^{-1})	k_2 (min^{-1})	k_3 (min^{-1})	k_4 (min^{-1})	V (unitless)	MSC (unitless)
Frontal cortex	0.08 ± 0.03	0.23 ± 0.09	0.14 ± 0.03	0.02 ± 0.01	4.7 ± 2.0	2.0 ± 0.4
	5.2 ± 0.7	18.0 ± 5.5	16.7 ± 9.0	9.4 ± 2.2	3.9 ± 1.4	
Temporal cortex	0.10 ± 0.03	0.36 ± 0.15	0.19 ± 0.05	0.01 ± 0.01	5.4 ± 1.8	1.4 ± 0.2
	7.4 ± 0.8	22.8 ± 7.6	18.0 ± 9.2	10.1 ± 2.9	4.7 ± 1.2	
Hippocampus	0.10 ± 0.06	0.52 ± 0.41	0.21 ± 0.10	0.01 ± 0.01	7.9 ± 2.2	1.0 ± 0.6
	9.3 ± 1.8	22.7 ± 6.9	16.4 ± 3.9	30.1 ± 33.4	23.4 ± 29.5	
Cerebellum	0.12 ± 0.12	0.49 ± 0.66	0.07 ± 0.06	0.01 ± 0.01	2.3 ± 1.7	2.1 ± 0.9
	7.6 ± 4.4	16.78 ± 2.1	25.3 ± 13.1	22.5 ± 7.1	8.2 ± 1.9	

V = distribution volume; MSC = model selection criteria; %COV is a measure of the identifiability of the associated parameter and is the mean ± SD of the standard error of the fits, expressed as a percentage of the rate constant itself; $n = 4$.

better fit to the data, and this difference was significant by F test in all regions of all subjects ($P < 0.001$). In the two-tissue compartment model, V was relatively well identified with COV values < 10% (Table I). However, individual rate constants k_2, k_3, and k_4 (but not K_1) showed poor identifiability with COV values > 10% in most regions (Table I).

Time stability of parameter estimates

The time stability of parameter estimation was analyzed for cerebellum and temporal cortex, a receptor-poor and receptor-rich region, respectively. The first two subjects were scanned for 120 min, and the calculated distribution volumes of cerebellum and temporal cortex continuously increased by about 30% from 60 to 120 min. To see whether the values stabilized at later times, the last four subjects were scanned for 150 min. Similar to the initial results, distribution volumes (V) of cerebellum and temporal cortex continuously increased from 90 to 150 min by 28% ± 14% and 25% ± 8%, respectively (Fig. 6A). The BP_1 in temporal cortex also continuously increased from 90 to 150 min by 25% ± 8%. In our previous experiment in monkey (Yasuno et al., 2006), the time stability of parameter estimation was analyzed for the cerebellum and four receptor-rich regions (prefrontal cortex, lateral temporal cortex, dorsal raphe, and medial temporal region) in scans of 120-min duration. We defined significant bias with the relatively strict criterion of >±5% of the value determined with the entire 120-min data set. No significant bias was found for distribution volumes in any target region or cerebellum for the durations > 70 min (Fig. 6B).

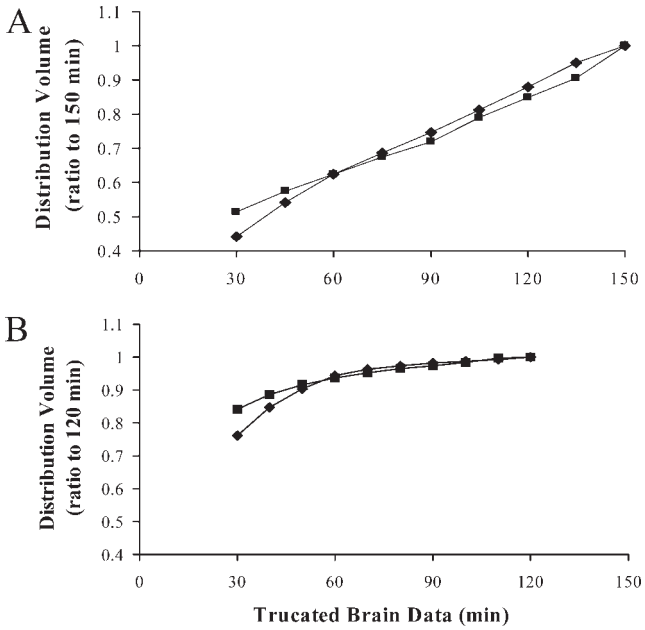

Fig. 6. Time stability of parameter estimation. Each point represents the estimated value from 0 to the specified time and is expressed as a % of the 150-min value in human and of 120 min in monkey. **A:** Relationship between distribution volumes obtained by two-tissue compartment model and experiment duration in cerebellum (■) and temporal cortex (◆) in human. **B:** Relationship between distribution volumes obtained by two-tissue compartment model and the experiment duration in cerebellum (■) and receptor-rich regions (◆) from our previous monkey data (Yasuno et al., 2006).

Effect of later plasma data on distribution volume

Distribution volume is the ratio at equilibrium of brain radioactivity to the concentration of parent radiotracer in plasma. Since this ratio increased with longer scan analysis, the time unstable distribution volume could have been caused by an abnormally large "numerator" (brain activity) or an inaccurately small "denominator" (parent radiotracer in plasma). As described earlier, we examined the effect of the "numerator" on distribution volume using increasingly truncated brain data but with the same complete plasma input function (0–150 min). To assess the effect of the "denominator," we used increasingly truncated plasma data but with same complete brain curve (0–150 min). When plasma data were decreased from 0–150 to 0–90 min, the plasma AUC decreased by only 6% ± 7% (Fig. 7A). Since plasma AUC is directly proportional to the peripheral clearance of the radiotracer, the analysis showed that clearance from 90 min of data was within 6% of the accuracy of that using 150 min of data. Furthermore, distribution

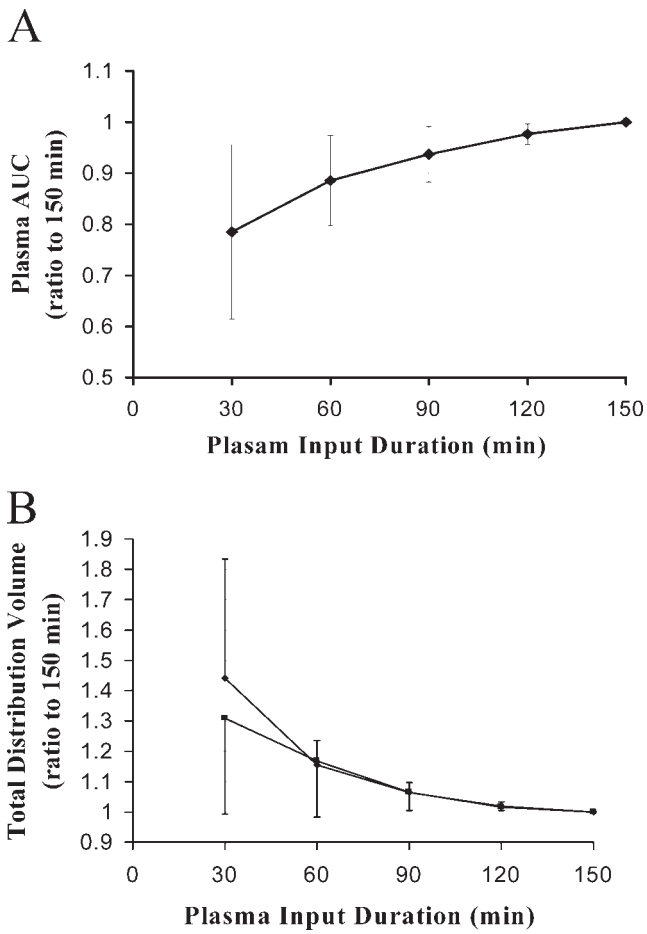

Fig. 7. Effect of later time points of plasma input on distribution volumes. Each point represents the estimated value from 0 to the specified time and is expressed as a % of the 150-min value; n = 6. **A:** Relationship between the plasma input duration and AUC (area under the curve). **B:** Relationship between the plasma input duration and distribution volumes obtained by two-tissue compartment model in cerebellum (■) and temporal cortex (◆).

volumes for cerebellum and temporal cortex increased by only 7% ± 7% and 6% ± 5%, respectively, with 0–90 min compared with 0–150 min data (Fig. 7B).

Reference tissue analysis

One possible way to overcome the time instability of distribution volume measurements using arterial plasma data is a reference tissue analysis. The time stability of BP of temporal cortex was estimated with the MRTM. BP of temporal cortex increased from 90 to 150 min by 19% ± 26%, but with greater intersubject variability than V or BP_1. For example, BP estimated at 120 min for the six subjects had an intersubject %COV of 36%, whereas V had 5% COV and BP_1 had 5% COV.

DISCUSSION

Brain uptake of [^{11}C](*R*)-(−)-RWAY in animals can be displaced by WAY-100635, indicating the binding is specific, saturable, and selective for 5-HT$_{1A}$ receptors (Liow et al., 2007; Yasuno et al., 2006). Therefore, we chose to evaluate [^{11}C](*R*)-(−)-RWAY in human subjects. Brain activity was higher in receptor-rich regions (e.g., frontal cortex, temporal cortex, and hippocampus) and had about three times the level in receptor-poor cerebellum at 80 min after tracer injection. However, the decline of brain activity in some individuals was slow, and we wondered whether this reflected a more serious problem.

Time instability of distribution volume

Perhaps the best way to determine if human brain washout is "too slow" is to compare it with the peripheral washout (i.e., clearance) of the parent radiotracer in each individual. That is, does the peripheral clearance of parent radiotracer suggest that the brain activity should wash out faster, if we assume that only parent radiotracer and no radiometabolites are in brain? This question can be answered by calculating the time stability of distribution volume, estimated with varying lengths of the brain data. Distribution volume is the ratio at equilibrium of activity in brain to the concentration of parent radiotracer in plasma. We estimated this equilibrium value from the ratio of rate constants (see Methods), using standard compartmental modeling methods. For the purposes of this study, distribution volume can also be understood as the ratio of the areas under the curve from time zero to infinity of the brain activity compared to plasma parent tracer.

$$V = \frac{\mathrm{AUC_{brain}}}{\mathrm{AUC_{plasma}}} = \frac{\int_0^\infty C_{\mathrm{brain}}(t)}{\int_0^\infty C_A(t)}$$

where $\mathrm{AUC_{brain}}$ refers to total activity in the region (specific and nondisplaceable); $\mathrm{AUC_{plasma}}$ refers to the total concentration (free plus protein bound) of the parent radiotracer separated from radiometabolites (Lassen, 1992).

Viewed from the perspective of a ratio of AUCs, the time instability of distribution volume V could reflect an error in brain measurements (e.g., the presence of a radiometabolite) or plasma measurements (e.g., inaccurate because low activity, especially at later time points). To assess the impact of brain measurements, we analyzed the time stability of the distribution volumes for cerebellum and one receptor-rich region (namely, temporal cortex) with a two-tissue compartment model. Distribution volumes were compared with reference values obtained with the complete 150-min data set. Distribution volumes for both human cerebellum and temporal cortex increased continuously from 90 to 150 min by 28% ± 14% and 25% ± 8%, respectively. In contrast, distribution volumes of monkey cerebellum increased by only 2–3% from 80 to 120 min (Yasuno et al., 2006). The time interval

for the monkey values was 40 min, and a comparable 40-min change of distribution volume for this human study would be 18%, which is still considerably higher than the 2–3% in monkeys.

Did errors in plasma measurements cause time instability?

Viewed as a ratio of AUCs, distribution volume is also vulnerable to measurement error and biological variations of the denominator (plasma input), especially at later time points. Hence, we investigated the effect of later plasma data on distribution volume by truncating the input durations from 0–150 to 0–30 min (Fig. 7). When the plasma input was truncated from 0–150 to 0–90 min, the plasma AUC decreased by only 6% ± 7% (Fig. 7A), and the distribution volumes for cerebellum and temporal cortex increased 7% ± 7% and 6% ± 5%, respectively (Fig. 7B). In contrast, truncation of the brain data (with no change in the complete arterial input function) increased distribution volume about 30% from 90 to 150 min in cerebellum and temporal cortex. Thus, errors in the plasma measurements, if they occurred, could not explain the magnitude of time instability of distribution volume determined from truncated brain data. If the plasma parent concentrations were accurately measured, then the decrease of the plasma AUC (and the corresponding increase in distribution volume) merely reflected a more accurate measurement of the total AUC with longer data sets. In fact, AUC and its pharmacological analog, clearance, are more accurately measured with a larger number of data points over longer time durations (Rowland and Tozer, 1994).

Radiometabolite(s) likely cause time instability

We suspect that humans generate a radiometabolite(s) that enter brain at a higher rate than that in monkeys. The radiochromatographic profile of [^{11}C](*R*)-(−)-RWAY in the monkey was different than that of the human (Fig. 5). Radiometabolite **3** is the most lipophilic radiometabolite and likely penetrates the blood–brain barrier. Ex vivo analysis of rat brain analysis at 30 min after injection of [^{11}C](*R*)-(−)-RWAY showed that a radiometabolite of similar HPLC retention was present in brain and represented 8% of total brain activity (Liow et al., 2007). Furthermore, radiometabolite **3** occurred at a higher percentage of total plasma activity in human (13.6% ± 6.4%) compared with monkey (5.9% ± 3.1%) at 10 min after tracer injection. However, we found no correlation between subjects on the rate of generating metabolite **3** and the time instability of distribution volume. As discussed later, more than one radiometabolite may enter human brain: one that does and one that does not bind to the 5-HT$_{1A}$ receptor.

We do not know the structure of radiometabolite **3** and had not expected it to be so apparently problematic in human subjects. (*R*)-(−)-RWAY was designed to be metabolically resistant compared with WAY-100635, and mass spectrometry confirmed the metabolic stability of its amide bond in rats (Shetty et al., 2005). Furthermore, imaging with [^{11}C](*R*)-(−)-RWAY in monkeys was quite promising. Stable values of distribution volume were obtained within ~60 min of imaging and increased by only 5% in the subsequent 60-min interval (Yasuno et al., 2006). The time instability in humans of distribution volume measurements was unexpected and may have been caused by a relatively low abundant radiometabolite previously detected in rat and monkey. Despite the logical design of a tracer with resistance to amide hydrolysis, another unanticipated metabolic path apparently foiled the utility of this radiotracer in humans.

Can anything other than accumulation of radiometabolites explain the time instability of distribution volume? We can think of only one other explanation: the parent radiotracer did not achieve "equilibrium" binding in brain within 150 min. We think this explanation is unlikely based on our prior studies of [^{11}C](*R*)-(−)-RWAY in monkeys. The time of "equilibrium binding" for PET receptor studies lacks consensus definition. Nevertheless, most researchers agree that equilibrium occurs close to the time of peak brain activity. In fact, brain activity of [^{11}C](*R*)-(−)-RWAY in both monkey and human occurred at the same time (~10 min). Furthermore, distribution volumes in monkey brain were remarkably stable from 70 to 120 min, showing that the ratio of kinetic rate constants were well defined with only 70-min data. Finally, the cerebellum has only a small number of 5-HT$_{1A}$ receptors, and its nondisplaceable uptake should reach equilibrium sooner than a receptor-rich region. Despite this fact, distribution volume for human cerebellum continuously increased from 90 to 150 min.

Was the putative radiometabolite active or inactive in brain? That is, did the proposed metabolite bind to the receptor or have negligible affinity? Our results demonstrated that the BP$_1$ continually increase in temporal cortex, suggesting that the metabolite might be active. However, if the metabolite was active, then it will have greater percentage effect on time instability of distribution volume in temporal cortex than cerebellum, since the former has more receptors. The opposite would be true if the metabolite is inactive. In fact, the time instability was quite similar in temporal cortex and cerebellum (Fig. 6A). Thus, these results have no clear implication for the receptor activity of the putative metabolite. Furthermore, both an active and an inactive radiometabolite could have entered the brain. Estimation of BP with reference tissue analysis is vulnerable to errors in both active (numerator) and inactive (denominator) radiometabolites. The ratio of active to inactive metabolites may be different among subjects. With variability of this ratio between subjects, the reference tissue BP would

show greater intersubject variability than V or BP_1. In fact, our results did show that BP had a high intersubject variability (36% COV).

Is [^{11}C](*R*)-(−)-RWAY a substrate for P-glycoprotein (P-gp) efflux from brain, and could that explain the temporal instability of distribution volume? The P-gp transporter is widely in the body and acts at the blood–brain barrier to block the entry of several diverse types of lipophilic compounds into the brain (Ambudkar et al., 1999). We previously found that [^{11}C](*R*)-(−)-RWAY is clearly a substrate for P-gp in rodent brain (Liow et al., 2007), but is unlikely to be a significant substrate in monkey brain (Yasuno et al., 2006). We do not know whether [^{11}C](*R*)-(−)-RWAY is a substrate for P-gp in humans, but such efflux would not explain the increase in distribution volume with time. P-gp effluxes drugs while in transmit through the endothelial membrane that effectively constitutes the blood–brain barrier. That is, P-gp decreases brain radioactivity of radioligands that are substrate. In contrast, we found higher brain activity levels than expected from the plasma concentration of parent radiotracer.

In conclusion, human brain activity of [^{11}C](*R*)-(−)-RWAY showed an unusually slow washout compared with that in monkeys and relative to the peripheral clearance of the radiotracer. The consequence of the latter was that distribution volumes in both 5-HT_{1A} receptor-rich and -poor regions were unstable and increased during the scan. This confounding effect precludes choosing any particular scan duration to reflect receptor density and may vary between individuals or between subject groups. The increasing distribution volume was unlikely due to the variation of plasma input at later time points, since the truncation of plasma time points from 150 to 90 min had relatively small effects on the plasma AUC. Taken together, we suspect that the slow washout and the instability of distribution volumes of [^{11}C](*R*)-(−)-RWAY are most likely due to the accumulation of radiometabolite(s) in brain. For these reasons, we are discontinuing use of [^{11}C](*R*)-(−)-RWAY in human subjects.

ACKNOWLEDGMENTS

X.-Y. Zhang is the recipient of the Clinical Pharmacology Research Associate Training Fellowship Award by National Institute of General Medical Sciences, NIH. We thank Janet Sangare, C-RNP, for subject recruitment and medical coverage, Robert Gladding, CNMT, for technical assistance, Jonathan Gourley for helping with arterial plasma analysis, the staff of the NIH PET Department for successful completion of the scanning studies, and PMOD Technologies for providing its image analysis and modeling software.

REFERENCES

Akaike H. 1974. A new look at the statistical model identification. IEEE Trans Automat Control AC 19:716–723.

Ambudkar SV, Dey S, Hrycyna CA, Ramachandra M, Pastan I, Gottesman MM. 1999. Biochemical, cellular, and pharmacological aspects of the multidrug transporter. Annu Rev Pharmacol Toxicol 39:361–398.

Bevington PR, Robinson DK. 2003. Data reduction and error analysis for the physical sciences. New York: McGraw-Hill.

Carson R. 1986. Parameter estimation in positron emission tomography. In: Phelps M, Mazziotta J, Schelbert H, editors. Positron emission tomography and autoradiography: Principles and applications for the brain and heart. New York: Raven Press. p 347–390.

Collins DL, Neelin P, Peters TM, Evans AC. 1994. Automatic 3D intersubject registration of MR volumetric data in standardized Talairach space. J Comput Assist Tomogr 18:192–205.

Cunningham V, Lammertsma A. 1995. Radioligand studies in brain: Kinetic analysis of PET data. Med Chem Res 5:79–96.

Giovacchini G, Toczek MT, Bonwetsch R, Bagic A, Lang L, Fraser C, Reeves-Tyer P, Herscovitch P, Eckelman WC, Carson RE, Theodore WH. 2005. 5-HT_{1A} receptors are reduced in temporal lobe epilepsy after partial-volume correction. J Nucl Med 46:1128–1135.

Gunn RN, Sargent PA, Bench CJ, Rabiner EA, Osman S, Pike VW, Hume SP, Grasby PM, Lammertsma AA. 1998. Tracer kinetic modeling of the 5-HT_{1A} receptor ligand [*carbonyl*-^{11}C]WAY-100635 for PET. Neuroimage 8:426–440.

Hawkins RA, Phelps ME, Huang S-C. 1986. Effects of temporal sampling, glucose metabolic rates, and disruptions of the blood–brain barrier on the FDG model with and without a vascular compartment: Studies in human brain tumors with PET. J Cereb Blood Flow Metab 6:170–183.

Ichise M, Liow JS, Lu JQ, Takano A, Model K, Toyama H, Suhara T, Suzuki K, Innis RB, Carson RE. 2003. Linearized reference tissue parametric imaging methods: Application to [^{11}C]DASB positron emission tomography studies of the serotonin transporter in human brain. J Cereb Blood Flow Metab 23:1096–1112.

Lang LX, Jagoda E, Schmall B, Vuong BK, Adams HR, Nelson DL, Carson RE, Eckelman WC. 1999. Development of fluorine-18-labeled 5-HT_{1A} antagonists. J Med Chem 42:1576–1586.

Lassen NA. 1992. Neuroreceptor quantitation in vivo by the steady state principle using constant infusion or bolus injection of radioactive tracers. J Cereb Blood Flow Metab 12:709–716.

Liow J-S, Lu S, McCarron JA, Hong J, Musachio JL, Pike VW, Innis RB, Zoghbi SS. 2007. Effect of P-glycoprotein inhibitor, cyclosporine A, on the disposition in rodent brain and blood of the 5-HT_{1A} receptor radioligand [^{11}C](*R*)-(−)RWAY. Synapse 61:96–105.

Osman S, Lundkvist C, Pike V, Halldin C, McCarron J, Swahn C-G, Farde L, Ginovart N, Luthra S, Gunn R, Bench C, Sargent P, Grasby P. 1998. Characterisation of the appearance of radioactive metabolites in monkey and human plasma from the 5-HT_{1A} recepeptor radioligand [*carbonyl*-^{11}C]WAY-100635: Explanation of high signal contrast in PET and aid to biomathematical modeling. Nucl Med Biol 25:215–223.

Parsey RV, Arango V, Olvet DM, Oquendo MA, Van Heertum RL, John Mann J. 2005. Regional heterogeneity of 5-HT1A receptors in human cerebellum as assessed by positron emission tomography. J Cereb Blood Flow Metab 25:785–793.

Pike VW, McCarron JA, Lammerstma AA, Hume SP, Poole K, Grasby PM, Malizia A, Cliffe IA, Fletcher A, Bench CJ. 1995. First delineation of 5-HT_{1A} receptors in human brain with PET and [^{11}C]WAY-100635. Eur J Pharmacol 283:R1–R3.

Pike VW, McCarron JA, Lammerstma AA, Osman S, Hume SP, Sargent PA, Bench CJ, Cliffe IA, Fletcher A, Grasby PM. 1996. Exquisite delineation of 5-HT_{1A} receptors in human brain with PET and [*carbonyl*-^{11}C]WAY-100635. Eur J Pharmacol 301:R5–R7.

Rowland M, Tozer TN. 1994.Assessment of AUC. In: Clinical pharmacokinetics: Concepts and applications, 3rd ed. Philadelphia: Lea and Febiger. p 469–472. Appendix 1-A Assessment of AUC, pp. 469–472.

Shetty H, Zoghbi S, McCarron J, Liow J-S, Hong J, Pike V. 2005. Characterization of in vivo rat metabolites of [*O-methyl*-^{11}C]RWAY by LC-MS. J Label Compd Radiopharm 48 (Suppl 1):278.

Yasuno F, Zoghbi SS, McCarron JA, Hong J, Ichise M, Brown AK, Gladding RL, Bacher JD, Pike VW, Innis RB. 2006. Quantification of serotonin 5-HT1A receptors in monkey brain with [^{11}C](*R*)-(−)-RWAY. Synapse 60:510–520.

Zoghbi SS, Shetty HU, Ichise M, Fujita M, Imaizumi M, Liow JS, Shah J, Musachio JL, Pike VW, Innis RB. 2006. PET imaging of the dopamine transporter with ^{18}F-FECNT: A polar radiometabolite confounds brain radioligand measurements. J Nucl Med 47:520–527.